Synergistic Effects of Crystal Phase and Strain for N_2 Dissociation on Ru(0001) Surfaces with Multilayered Hexagonal Close-Packed Structures

Tuanping Xie, Jing Zhou, Li Cai, Wangyu Hu, Bowen Huang, and Dingwang Yuan*

Read Online

ACCESS | Metrics & More | Article Recommendations | SI Supporting Information

ABSTRACT: The synergistic effects of strain and crystal phase on the reaction activity of nitrogen molecule dissociation have been studied using density functional theory calculations on Ru(0001) surfaces with multilayered hexagonal close-packed structures. The phase transformation from hexagonal close-packed phase (2H) to face-centered cubic (3C) phase or unconventional phases (4H, DHCP, $6H_1$, and $6H_2$) would occur under the uniaxial tensile strain loaded along the c axis. The close-packed surfaces of unconventional crystal phases show an enhanced chemical reactivity for N adsorption due to the upshifted d-band center of Ru. However, the N_2 adsorption energy is almost independent of the applied strain and crystal phase. The optimized catalytic activity of Ru(0001) surfaces with the unconventional phases is found for the N_2 dissociation through breaking the scaling relationships between the reaction barrier and reaction energy. Our results indicate that the strain-induced phase transformation is an effective method to improve the catalytic activity of noble metal catalysts toward the N_2 dissociation reaction.
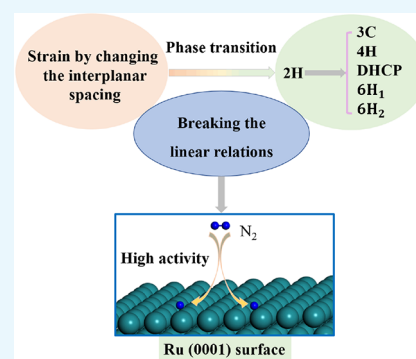
INTRODUCTION

Ammonia is indispensable as a fertilizer feedstock, chemical synthesis precursor, and carbon-free energy carrier.[1] However, there exist harsh reaction conditions, high energy consumption, and a great amount of greenhouse gas emissions for the century-old Harber−Bosch process (HBP), which synthesizes ammonia from hydrogen and nitrogen over Fe-based catalysts.[2−4] One promising approach is electrochemical ammonia synthesis via the nitrogen reduction reaction (NRR) under ambient conditions, which can not only avoid the deficiencies of the HBP but also enable a sustainable process for making fertilizers and energy carriers.[5,6]

However, it is plagued by both the low selectivity of ammonia formation (also known as Faradaic efficiency) due to the competing hydrogen evolution reaction and the low yield rate owing to the highly stable N_2 on elemental metal surfaces.[7,8] Besides Fe-based catalysts, ruthenium (Ru) catalysts supported on carbon were developed as second-generation catalysts for NH_3 synthesis.[9] In order to use ruthenium more economically and sustainably, many studies have been done to improve the catalytic activity and selectivity of ruthenium toward the NRR. It was reported that the catalytic activity of Ru depends on the size of the Ru nanocrystals as well as the geometric configuration and charge state of the reactive sites for N_2 activation during the key reaction step for NH_3 synthesis.[10,11] For instance, the special type of B_5 step sites in Ru nanoparticles is the active centers for N_2 dissociation at low temperature.[12,13] Using electron

microscopy characterization and density functional theory (DFT) calculations, C. J. H. Jacobsen et al. reported Ru nanocrystals with size ranging from 1 to 2 nm have the greatest proportion of active sites for N_2 dissociation.[10] Also, the activity of Ru catalysts was significantly enhanced by electron injection from alkali or alkaline earth metal oxide promoters through improving the charge transfer from the eletron-rich Ru to the antibonding π^*-orbitals of N_2.[14]

In addition, both the strain and crystal phase engineering have been successfully used to tune the catalytic performance of precious metal nanomaterials in recent years.[15−17] Applied surface strain has been proved to be an efficient approach to enhance the reactivity of the metal surface through regulating the electronic structures (e.g., the width and position of the metal d-band) in the pioneering works of J. K. Nørskov et al.[18,19] Experimentally, the surface strain of catalysts can be induced by growing epitaxial metal overlayers on substrate due to lattice mismatch, which makes it feasible to synthesize metal nanocrystals with new crystal phases, e.g., Ru catalytsts with a face-centered cubic (*fcc*) phase.[20,21] Generally, the *fcc* and hexagonal close-packed (*hcp*) structures are also known as 3C

and 2H, where the Arabic number refers to the number of atomic planes in a stacking sequence and the "C" and "H" represent the cubic Bravais lattice and hexagonal Bravais lattice, respectively.[22] Besides 2H structures, there are some other multilayered hexagonal close-packed structures with a longer packing period, namely unconventional phases, such as ABCBABCB(4H), ABACABAC(DHCP), ABCACBABCACB-($6H_1$), and ABCBABABCBAB($6H_2$), which have been reported in some noble metal (e.g., Ru, Os, Rh, Ir, Pd, Pt, Ag, and Au) nanomaterials.[23]

Recently, considerable progress has been made in the phase engineering of nanomaterials (PEN), including the synthesis of nobel metal nanomaterials with unconventional phases under mild conditions.[15] For example, Yao et al. reported both *fcc* and hexagonal close-packed (*hcp*) Ru can be selectively grown through varying the lattice spacing of the Pd−Cu substrate along the [100] and [010] directions of the $PdCu_3(001)$ surface.[24] And also, Fan et al. crystallized Ru in the 4H/*fcc* structure via the process of wet chemical epitaxial deposition on a Au nanoribbon template.[25] In this process, the lattice (i.e., interplanar spacing) mismatch between Au and Ru induces an epitaxial strain in the close-packed $[0001]_h$ direction of the hexagonal lattice, which results in partial phase transformation among the *fcc*, 2H, and 4H phases. The *d*-band model theory has been successful in explaining the impact of strain for catalytic performance.[18,26] This means that we can adjust some properties, especially the catalytic property, of noble metal nanomaterials by the crystal phase, because different crystal phases have different atomic arrangements and then modify their electronic structure.[16,27,28] As known, the compressive (tensile) strain can downshift (upshift) the *d*-band center of the metal surface and then weaken (strengthen) the adsorbate−surface interaction.[29] However, the synergistic effects of the surface strain and crystal phase on the catalytic properties of noble metals with nontraditional crystal structures have not yet been clearly clarified, and theoretical studies are therefore required to attain comprehensive understandings.

It is worth noting that unconventional nanocrystals of Ru have been successfully synthesized, including the *fcc*[30] phase and 4H[31] phase, which present excellent catalytic performance in some typical catalytic reactions. For example, during the Fischer−Tropsch (FT) synthesis, the *fcc*-Ru catalyst has a higher activity than the *hcp*-Ru catalyst because of a high density of active sites in the *fcc*-Ru nanoparticles.[32] Yao Zheng et al. found that the *fcc*-Ru nanoparticles synthesized on C_3N_4 have better hydrogen evolution reaction (HER) activities than the Ru/C and Pt/C under alkaline conditions owing to a lower dissociation energy barrier toward water and hydrogen.[33] Given the high catalytic efficiency of the unconventional crystal phases of Ru reported in the available experiments, further study is needed to understand the mechanism of the strain-induced phase transformation from 2H to the typical unconventional crystal phases by DFT calculation and then design new Ru catalysts with phase-dependent catalytic activity for the N_2 molecule dissociation reaction.

In this article, we present the results of strain-induced phase transformation of Ru from 2H to novel crystal structures and the catalytic activity of Ru(0001) surfaces with multilayered hexagonal close-packed structures toward N_2 dissociation using DFT calculations. We first focus on the stability of Ru crystal phases with applying a certain biaxial strain along the *a* and *b* directions and uniaxial strain along the *c* axis, and we found

that the applied uniaxial strain along the *c* axis will facilitate the phase transformation from 2H to 3C and the unconventional phases (4H, DHCP, and 6H). Compared to the 2H Ru(0001) surface, the Ru(0001) surfaces of the unconventional phases show higher catalytic activity for N_2 dissociation, which is attributed to the enhanced N adsorption energies and the broken scaling relationships in the N_2 dissociation process.

■ RESULTS AND DISCUSSION

Stability of Unconventional Ru Crystal Phases under Strain. With DFT calculations, first, we obtained the equilibrium crystal structures of 2H, 3C, 4H, DHCP, $6H_1$, and $6H_2$. The detailed lattice parameters and the atomic arrangements of unit cells are shown in Table 1 and Figure 1,

Table 1. Lattice Constants (*a*, *c*), Interplanar Spacing (*d*), *d/a* Ratio, and Binding Energy (E_b) of Ru with the Stable State 2H and Multilayered Hexagonal Close-Packed Structures

| structure	*a* (Å)	*c* (Å)	*d* (Å)	*d/a*	E_b (eV/atom)
2H	2.689	4.272	2.136	0.794	−8.547
3C	2.665	6.544	2.179	0.818	−8.435
4H	2.685	8.613	2.153	0.802	−8.471
DHCP	2.685	8.614	2.153	0.802	−8.471
$6H_1$	2.684	12.929	2.155	0.803	−8.474
$6H_2$	2.683	12.863	2.144	0.799	−8.509
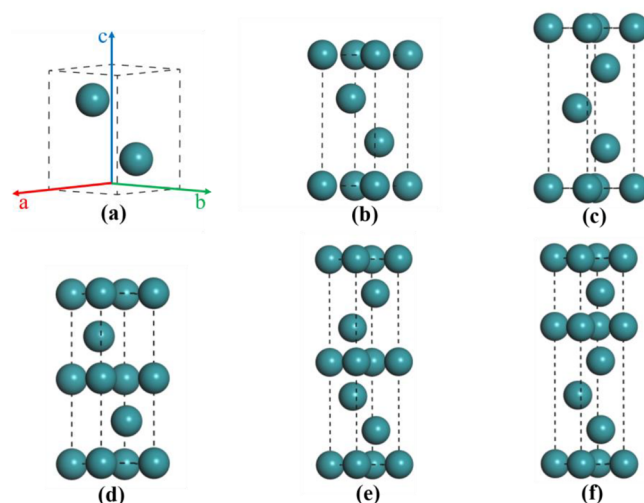
Figure 1. Unit cells of six crystal structures, including 2H, 3C, 4H, DHCP, $6H_1$, and $6H_2$, for noble metal Ru. The detailed lattice parameters are shown in Table 1.

respectively. For the equilibrium crystal structures, the order of stability (binding energy per atom) is 2H > $6H_2$ > $6H_1$ > 4H = DHCP > 3C, and the relative energies are 38, 73, 76, and 113 meV for $6H_2$, $6H_1$, 4H/DHCP, and 3C, respectively, referring to the 2H structure. Compared to the other multilayered hexagonal close-packed structures, *fcc* Ru is energetically less favorable at the equilibrium phase (see Table 1). However, Ru nanoparticles trend to the phase transformation from 2H to 3C or 4H under the epitaxial strain over PdCu substrates[24] or 4H Au nanoribbons.[25] Therefore, to unveil the strain-induced phase transformation behavior of 2H Ru, we will systematically study the strain modulation of Ru phase transformation from

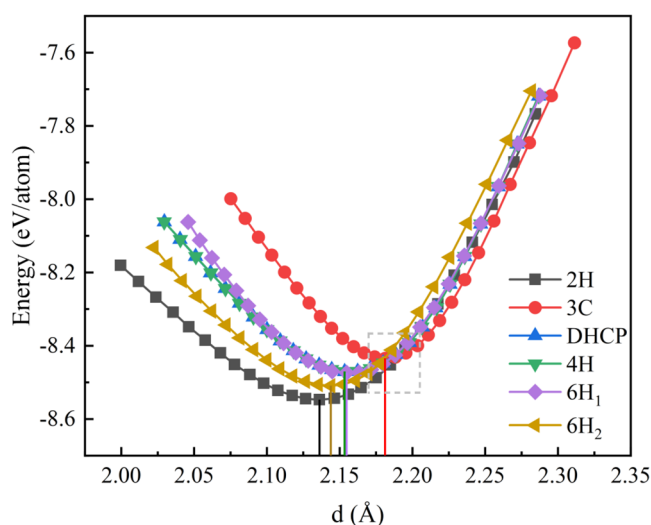2H to the unconventional crystal phases under strain in the following.

In the epitaxy growth, the phase structures of metal overlays depend on the extent of the lattice mismatch and the crystal plane orientation of the substrate template.[34] Therefore, first, we considered the effects of biaxial strain acting on the basal plane of the 2H hexagonal lattice by varying the lattice parameters within −0.26 Å (negative values represent compressive strain) to +0.26 Å (positive values refer to tensile strain) along the a and b directions, shown in Figure 2.
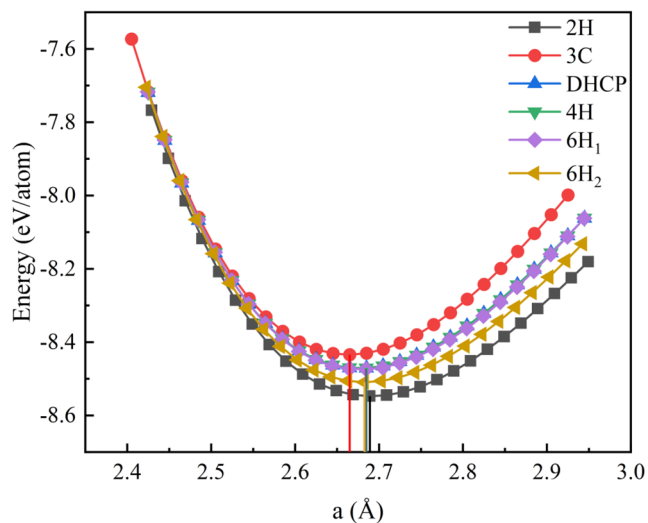
Figure 2. Energy per atom as a function of the length of the a (or b) axis. The vertical and horizontal lines represent the stable state values. The calculated details are given in the Supporting Information.

According to Figure 2, with the increase of tensile strain, the stability order of different Ru crystal phases remains unchangeable compared to the equilibrium structures, but the energies of the Ru crystal phases are going to be evidently different from each other. In the equilibrium structures, the unconventional phases have larger interplanar spacings than the 2H phase (see Table 1). Due to the Poisson effect, the hexagonal Ru tends to compression in c directions perpendicular to the direction of tensile biaxial strain, shown in Figure S2, which makes further instability in the energy of the unconventional phases. On the contrary, the compressive strain could cause the increasing of the interplanar spacings, and there are no significant differences among the energies of all the crystal phases after loading a large compressive strain, similar to the strain-induced phase behavior of HCP, FCC, and 4H gold.[35] So, the phase transformation from 2H to the unconventional phases (3C, 4H, DHCP, and 6H) would happen with difficulty under the applied biaxial strain.

Next, we consider the impact of uniaxial strain on the stability of Ru with multilayered hexagonal close-packed structures, through changing the interplanar spacings of the (0001) lattice plane (the calculated details are presented in the Supporting Information). The relationship between energy and interplanar spacing is illustrated in Figure 3. It is worth noting that with the interplanar spacing increase or decrease (i.e., the uniaxial tensile strain or compressive strain), the relative stability of the considered crystal phases shows significantly different behaviors. In the region of compressive strain, the 2H phase is the most stable structure, and significant energy

Figure 3. Energy per atom as a function of the interplanar spacing. The vertical lines represent the stable state values. A partial enlargement of the gray dotted box is shown in Figure S3.

differences for the unconventional crystal phases occur at the less interplanar spacing referring to the 2H phase. The equilibrium interplanar spacings of 2H and 3C are 2.136 Å (minimum value) and 2.179 Å (maximum value), respectively, while the values of other crystal phases are similar to each other (2.153, 2.153, 2.155, and 2.144 Å for 4H, DHCP, $6H_1$, and $6H_2$, respectively). The interplanar spacings of 2H and 3C are marked in Figure 3 by black and red solid vertical lines, and the deviation between them is about 0.043 Å. Therefore, at a smaller interplanar spacing, the 2H phase should remain highly stable. It is worth mentioning that the unconventional crystal phases are comparable in energy with the 2H phase at the uniaxial tensile strain, and the 3C structure is transformed to the most stable phase beginning at d = 2.190 Å (see Figure S3), which indicates that a certain amount of uniaxial tensile strain can make the phase transition between 2H and 3C. Experimentally, 4H and 3C Ru were template synthesized through changing the interplanar distance of the close-packed planes in the [001] direction on the substrates of 4H Au nanostructures.[25] Therefore, the large interplanar spacing can promote the phase transformation of 2H to 3C and other long stacking period structures.

As we know, the close-packed structures (i.e., 2H, 3C, 4H, and 6H) have identical interlayer spacings along the stacking direction between neighboring atomic sheets, and the ideal ratio of interlayer spacing to in-plane bond length (i.e., d/a) is $\sqrt{2/3}$ = 0.816. Due to the effects of atomic d-band filling, phase structures, and strain (or pressure),[13,36,37] the actual d/a ratio generally deviates from the ideal value. Therefore, we calculated the d/a ratios of different Ru phases in the equilibrium structures, shown in Table 1, and present the energy as a function of d/a ratio for the deformed Ru with traditional and nontraditional crystal structures in Figure 4. For the equilibrium crystal structures, 2H has the lower d/a ratio (0.794), but 3C has the highest value (0.818), which is very close to the ideal ratio. Under strain conditions, the unconventional phases approach the 2H phase with a smaller energy difference (below 30 meV) when the d/a ratio is greater than 0.86. The d/a ratio is linearly related to the interlayer spacings (see Figure S4), and therefore, the phase
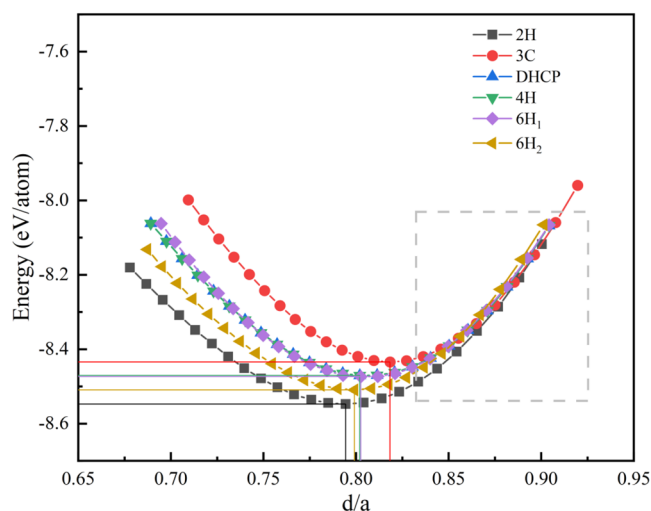
Figure 4. Energy per atom as a function of the d/a ratio value. The vertical and horizontal lines represent the stable state values. A partial enlargement of the gray dotted box is shown in Figure S5.

transformation of 2H can easily occur under an enhanced d/a ratio by adjusting the interplanar spacing of the (0001) lattice plane.

The phase transformations among the 2H, 3C, 4H, and 6H structures were reported through the shockley partial dislocations gilding mechanism.[20] To further discuss the phase stability of Ru crystals, we calculated the energy barrier per atom for a transformation involving the motion of close-packed layers for the 2H phase and the different nontraditional crystal structures using the solid state Nudged Elastic Band (ssNEB) method.[38−40] The transformation of 2H to 6H shows a low energy barrier. Moreover, the tensile strain can significantly promote these phase transformations with reduced barriers (see Table 2). Therefore, we proposed that the adjustment of the interplanar spacing or d/a ratio is an effective strategy to modulate the phase structures of Ru.

Table 2. Calculated Barrier of the Phase Transition from 2H to 3C, 4H, DHCP, $6H_1$, and $6H_2$ under the Equilibrium State and Strained State (d = 2.19, d/a = 0.86)^a

	equilibrium structures	d = 2.19	d/a = 0.86
2H → 3C	0.700	0.600	0.512
2H → 4H	0.766	0.672	0.571
2H → DHCP	0.766	0.672	0.571
2H → $6H_1$	0.671	0.577	0.476
2H → $6H_2$	0.641	0.610	0.446

^{a}All the values are in eV.

Adsorption of N Atom and N_2 Molecule. Crystal phase and strain engineering are the effective means to enhance the activity and selectivity of catalysts.[18,21,41,42] The 3C and 4H Ru nanoparticles are promising catalysts in several electrocatalytic reactions, such as the NRR, HER, and oxygen evolution reaction (OER).[23,43] The applied strain inevitably induces some changes in the packing patterns, interatomic interaction, atomic displacements, and potential defects in the crystals. Further, we will discuss the synergistic effects of the crystal phases and strain for N_2 adsorption and dissociation on the Ru(0001) surfaces with multilayered hexagonal close-packed structures.

According to the arrangements of close-packed atomic sheets of different unusual Ru crystal phases, the Ru(0001) surfaces have two types of terminal structures, denoted $(0001)_h$ and $(0001)_c$, which are similar to the atomic arrangements of the fcc (111) and 2H (0001) surfaces, respectively. In order to get insights into the effect of strain and the novel crystal on the electronic properties, we calculated the d-band center and partial density of state (PDOS) of Ru(0001) surfaces for the novel phases and tensile strain 2H (see Table S1 and Figure S4 in the Supporting Information). The strain in the metal surface could alter the d-bandwidth and shift its position relative to the Fermi level.[18,44] The tensile strain applied along the lateral direction of surface can narrow the d-band, shift the d-band center up, and enhance the bonding strength of an adsorbate on the surface.[29] We first consider the strain effects on the d-band position of 2H Ru. At larger interplanar spacing (i.e., compressive strain in close-packed atomic sheets), a wider d-band of Ru is found, and the position of the d-band center is shifted down (see Figure S4). Moreover, there is a linear relationship between the position of the d-band center and the interplanar spacing of the close-packed atomic plane for the strained 2H Ru (see Figure 5).
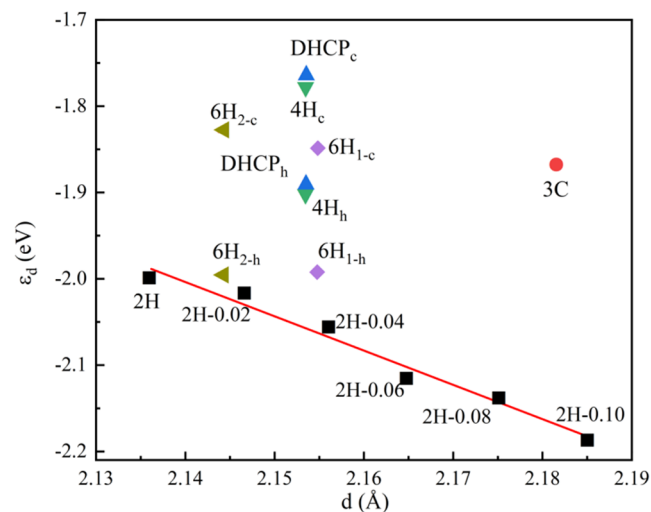
Figure 5. Correlation between the d-band center (ϵ_d) and atomic interplanar spacing of the (0001) surface (d) of the compressively strained 2H structures and unconventional crystal structures. h and c represent different terminal structures. The black square dots represent stable state 2H (marked in the figure) and compressive strained state 2H, which include 2H-0.02, 2H-0.04, 2H-0.06, 2H-0.08, and 2H-0.10. The number behind the "2H" means the compression strain value along the a (b) direction.

However, for the novel crystals, the d-band centers are evidently dependent on the crystal structures and are higher than the one of 2H at the same interplanar spacing. For instance, the d-band center of $6H_1$ is the highest. Therefore, the tensile strain along the c axis can cause the phase transformations from 2H to the unconventional phases and further might optimize the intrinsic electronic properties of Ru catalysts with a high activity for the adsorption and dissociation of the N_2 molecule.

Herein, we calculated the N_2/N adsorption on Ru(0001) surfaces with multilayered hexagonal close-packed structures. The adsorption energy of N_2 and N was defined as

$$E_{ad} = E_{adsorbate/slab} - E_{adsorbate} - E_{slab} \quad (1)$$

where $E_{adsorbate/slab}$ and E_{slab} are the total energies of the slab with and without adsorbates, respectively, and $E_{adsorbate}$ is the energy of the N_2 molecule or N atom in the gas phase. Under this definition, a lower (more negative) E_{ad} value means a stronger interaction between the adsorbate and surface and vice versa. The adsorption energies of the most stable adsorption states of N_2 molecules and N atoms on the Ru(0001) surfaces with multilayered hexagonal close-packed structures and strained 2H phases are listed in Table 3, where

Table 3. Calculated Adsorption Energies of Nitrogen Atom and Nitrogen Molecule, $E_{ad}^{N_2}$ and E_{ad}^{N} (in eV), Bond Distance between the Ru Atom in the Surface and the N Atom Belonging to the Adsorbed Nitrogen, $d_{Ru-N}^{N_2}$ (in Å), Bond Length of the Nitrogen Molecule in the Transition State, l_{N-N}^{TS} (in Å), and Dissociative Barrier of N_2, E_a (in eV)[a]

	$E_{ad}^{N_2}$	E_{ad}^{N}	$d_{Ru-N}^{N_2}$	E_a	l_{N-N}^{TS}
3C	−0.768	−6.438	1.954	1.511	1.706
4H	−0.789	−6.304	1.979	1.896	1.731
	(−0.764)	(−6.419)	(1.959)	(1.542)	(1.703)
DHCP	−0.763	−6.417	1.959	1.546	1.710
	(−0.763)	(−6.416)	(1.960)	(1.545)	(1.704)
$6H_1$	−0.751	−6.244	1.978	1.869	1.739
	(−0.770)	(−6.443)	(1.952)	(1.508)	(1.707)
$6H_2$	−0.821	−6.305	1.969	1.888	1.739
	(0.766)	(−6.436)	(1.961)	(1.555)	(1.706)
2H-0.00	−0.773	−6.332	1.970	1.811	1.732
2H-0.02	−0.774	−6.270	1.970	1.835	1.732
2H-0.04	−0.779	−6.210	1.965	1.861	1.733
2H-0.06	−0.777	−6.142	1.962	1.889	1.730
2H-0.08	−0.768	−6.069	1.956	1.918	1.733
2H-0.10	−0.766	−6.004	1.945	1.942	1.729

[a]Results in parentheses are the adsorption energies on Ru $(0001)_c$ surfaces.

the adsorption energies of N on the (0001) surfaces of 2H and 3C are close to the reported values,[43] and the corresponding adsorption geometries are also given in Figure S7. As for the strained surfaces of the 2H crystal phase, the more tensile strain (larger interplanar spacing) is imposed, the lower the d-band center the surfaces have, which means a weak adsorbate–surface interaction (higher adsorption energy). In Figure 6, a linear relation is found between the d-band center and the N adsorption energy on the 2H strained surfaces, which is similar to the behavior of oxygen atom adsorption on the strained Ru surfaces.[18] So, this means that the tensile strain along the c axis will cause a higher adsorption energy (less negative) of N atom and then weaken the Ru–N interaction on the 2H Ru(0001) surface. For the unconventional close-packed surfaces, the enhanced adsorption energies of N atom are shown in Figure 6 and Table 3 compared to the strained 2H Ru(0001) surfaces, which agrees with the character of the d-band center shown in Figure 5. Thus, the tensile strain along the c axis of 2H Ru has a negative effect on the activity of Ru(0001) toward N adsorption. But once the phase transformations occur from 2H to 3C, 4H, and 6H induced by the tensile strain along the c axis, Ru shows a higher chemical reactivity for N adsorption. And also, according to Figure 6, we note that the $(0001)_c$ surfaces of the 4H and 6H phases show higher catalytic reactivity than the other considered Ru(0001) surfaces for the
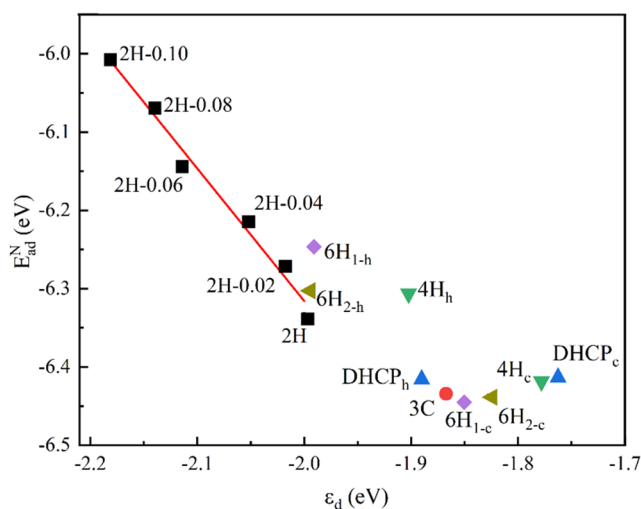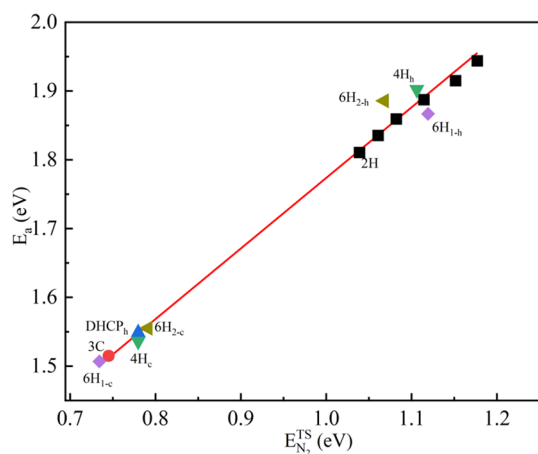

Figure 6. Nitrogen atom adsorption energy (E_{ad}^{N}) as a function of the d-band center (ϵ_d) for the compressively strained 2H structures and unconventional crystal structures. The red line was fitted using the data for 2H structures.
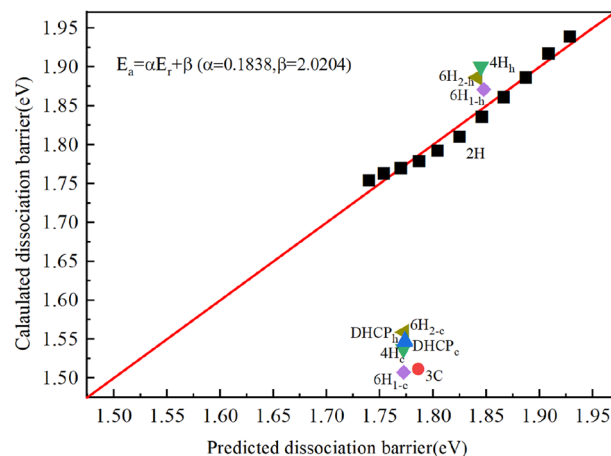
adsorption energies of N atom. For example, N atom on $(0001)_c$ of the $6H_1$ surface has the lowest adsorption energy with the value −6.443 eV.

Generally, the interaction between N_2 and metal surfaces can be described by a three-orbital interaction model[45] and the typical Blyholder model[46] with a synergism between σ-donation and π-back-donation. Due to the weak coupling between 5σ and $2\pi^*$ of the N_2 molecule with Ru-d states, comparing the strong hybridization between N-$2p$ and Ru-d, the N_2 molecule has low adsorption reactivity on Ru surfaces.[47] Here, we found that N_2 prefers to bind to the on-top site of Ru(0001) surfaces with a perpendicular geometry on the unconventional phases and 2H structures (see Figure S7). The adsorption energy of N_2 is −0.773 eV on the 2H Ru(0001) surface, which is slightly higher than the previous calculated results (−0.61 eV)[43,47] after including the correction of the vdW interaction. It shoud be noted that the N_2 adsorption energy is almost strain independent for the 2H structure. Moreover, due to the low chemical reactivity, the crystal structures have a minor impact on the adsorption energy of the N_2 molecule (see Table 3). The different effects of stain and crystallographic structure on the adsorption of N_2 and N atom would further change the transition state scaling relation[48] and Brønsted–Evans–Polanyi (BEP) relation[49] in the N_2 dissociation reaction.
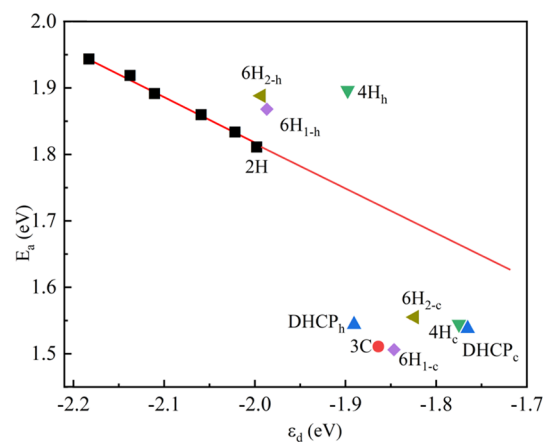
N_2 Dissociation. Finally, we discuss the dissociation of N_2 on the Ru(0001) surfaces with the strained 2H structures and other unconventional crystal phases. On a flat surface of Ru(0001), first, N_2 adsorbs on the atop site of a Ru atom vertically, and then the N_2 molecule will lie down and be parallel to the surface to be ready for the decomposition process.[47,50] The geometric configurations and energy profiles of the N_2 dissociation processes on the considered Ru(0001) surfaces are shown in Figure S7, while the scaling relationships of the reaction barriers (E_a) versus the N_2 adsorption energy in the transition state (E_{ad}^{TS}), reaction barriers (E_a) versus the d-band center (ϵ_d), and reaction barriers (E_a) versus the reaction energy (ΔE), i.e., the BEP relation, are shown in Figure 7, Figure 8, and Figure 9, respectively. The reaction energy (ΔE) and the activation barrier (E_a) were calculated as

Figure 7. Correlation between the adsorption energy of N_2 in TS ($E_{N_2}^{TS}$) and the dissociation barrier of N_2 (E_a) for the compressively strained 2H structures and unconventional crystal structures.

Figure 8. N_2 dissociation barrier (E_a) as a function of the d-band center (ϵ_d) for the compressively strained 2H structures and unconventional crystal structures. The red line was fitted using the data for 2H structures.

$$\Delta E = E_{FS} - E_{IS} \quad (2)$$

$$E_a = E_{TS} - E_{IS} \quad (3)$$

where E_{IS}, E_{TS}, and E_{FS} are the energies of the initial state (IS), the transition state (TS), and the final state (FS), respectively.

Generally, the transition state (TS) adsorption energy tends to be correlated to that of the initial state (IS) determined by the scaling relations. A more reactive metal would bind adsorbates in the TS more tightly; then the adsorbates in the IS are also bound more tightly. Therefore, the barriers of the dissociation reaction of small molecules are only slightly changed by changing the adsorption reactivity of metal surfaces.[41] However, as mentioned above, the stain for 2H Ru and crystal structures of Ru with hexagonal close-packed structures cannot evidently change the chemical activity of Ru(0001) surfaces for the weakly adsorbed N_2 molecule but can cause a significant increase for the adsorption energy (up to ∼1.0 eV) of the dissociative N_2 in the FS (see Table S2). The bond length of N_2 is stretched to ∼1.7 Å in the transition state (see Table 3), and then the strong interaction between Ru and N atoms results in the broadened N-2p states (see Figure S8). The electronic character of N_2 in the TS is very

Figure 9. Relationship between the predicted dissociation barrier and calculated dissociation barrier of N_2 dissociation for the strained 2H structures and unconventional crystal structures. The predicted dissociation barrier was calculated by the BEP relationship of strained 2H structures, that is $E_a = \alpha E_r + \beta$ ($\alpha = 0.1838$, $\beta = 2.0204$). E_a and E_r represent the dissociation barrier and reaction barrier, respectively.

similar to the adsorbed N atom (see Figure S9).[47] There are no adsorption-energy scaling relations, e.g., E_N vs $E_{N_2}^{IS}$, $E_{N_2}^{IS}$ vs $E_{N_2}^{TS}$, $E_{N_2}^{IS}$ vs $E_{N_2}^{FS}$ (see Figure S10, Figure S11, and Figure S12), but the stability of N_2 in the FS linearly depends on the interaction strength of N atom with Ru surfaces (see Figure S13). Therefore, the dissociation barrier of N_2 will be mainly related to the stability of N_2 in the TS or N atom's adsorption energy (see Figure 7 and Figure S14). In particular, a linear relationship is shown in Figure 7 between the adsorption energy of N_2 in the TS and the energy barrier of N_2 activation. Different from the linear scaling relation between the N adsorption energy and N_2 adsorption energy in the FS (shown in Figure S13), the N adsorption energy cannot be used as a good descriptor to determine the N_2 dissociation barrier and N_2 adsorption in the TS for unconventional crystal phases (shown in Figure S14 and Figure S15) . Compared to the 2H phase, some unconventional crystal phases can significantly reduce the activation barrier of N_2 through stabilizing the transition state of N_2 dissociation (see Figure 7).

To analyze the effects of electronic properties on the N_2 dissociation barrier, we further discuss the dependence between the barrier and the d-band center of Ru (see Figure 8). J. K. Nørskov et al. reported that the d-band center is a good descriptor for the reactivity (including adsorption energies and activation barrier of molecules) of the strained metal surfaces.[18] In multilayered hexagonal close-packed structures, the arrangements of the close-packed atomic layers can significantly change the electronic features of Ru's d states, and then the up-shifted d-band center of Ru can cause a stronger binding of N atom. Therefore, the energy barrier of N_2 activation is also related to both the applied stain and crystal structures of Ru. The larger interplanar spacing of the 2H phase can result in a lower chemical activity for N_2 activation with down-shifted d-band centers (see Table 3 and Figure 8). The crystal phases can upshift the d-band centers and then reduce the barriers of N_2 dissociation to below 1.5 eV, which is less than 1.8 eV on the stable 2H Ru(0001) surface. However, there is no linear relationship between the d-band center and N_2 dissociation barrier for the

Ru(0001) surfaces with unconventional crystal phases when comparing the strained 2H Ru(0001) surfaces (see Figure 8). Therefore, the N_2 dissociation barrier on Ru(0001) surfaces with multilayered hexagonal close-packed structures can be reduced through a synergistic role of crystal phases and strain (i.e., the strain-induced phase transformation between 2H and unconventional crystal phases (3C, 4H, DHCP, and 6H).

To change the catalytic activity and selectivity of catalysts, it is an effective strategy to break the scaling relations, especially the BEP relation describing correlations between reaction barriers and reaction energies, on the strained metal surfaces,[51] alloy surfaces,[52] and single-atom catalysts.[53] Moreover, constrained by the BEP relation, there is a contradiction between the molecular activation barrier and the adsorption energy of the intermediate species in the process of making ammonia from nitrogen by transition metal catalysts.[53] As mentioned above, on the strained 2H Ru(0001) surfaces, the catalytic properties including N atom adsorption and dissociation of N_2 can be well described with the scaling relations. In Figure 9, we fitted the linear relationship between reaction energy and the barrier of N_2 dissociation, i.e., the Brønsted−Evans−Polanyi relationship (BEP),[49] including only the energies on the strained 2H Ru(0001) surfaces. Under the limit of scaling relations, the tensile strain (at larger interplanar spacing) of 2H will give rise to a weak interaction between 2H Ru(0001) and the adsorbed N_2 in the TS or FS, and then a higher barrier is predicted according to the BEP relationship (see Figure S16). However, for unconventional crystal phases, this BEP relation cannot be used to describe the activation energy of N_2 dissociation, and the predicted barriers with the BEP relation are far higher than the DFT calculated values for the 3C, 6H, and 4H Ru(0001) surfaces. Experimentally, 3C Ru was obtained by applying a certain tensile strain to 2H Ru. Therefore, our results indicate that the synergistic effects of strain and crystal phase would be a better method to modulate nitrogen decomposition by breaking the linear scaling relations between energies of adsorbates.

CONCLUSIONS

In conclusion, we have systematically studied the synergistic effect of strain and crystal phase on nitrogen molecule decomposition on Ru(0001) surfaces with multilayered hexagonal close-packed structures. We found the applied uniaxial strain along the c axis will facilitate the phase transformation from 2H to the unconventional phases (3C, 4H, DHCP, and 6H), compared to the biaxial strain applied along the a and b directions. Specifically, a large interplanar spacing of close-packed atomic sheets can promote the phase transformation of 2H to 3C and other long stacking period structures. Once the phase transformations occur from 2H to 3C, 4H, and 6H, the close-packed surfaces of unconventional crystal phases show an enhanced chemical reactivity for N adsorption due to the upshifted d-band center of Ru. However, the N_2 adsorption energy is almost independent of applied strain and crystal structure for the multilayered hexagonal close-packed Ru(0001) surfaces. Notably, the strain-induced phase transformation among 2H and unconventional crystal phases is an effective strategy to break scaling relationships in the N_2 dissociation reaction. The N_2 dissociation barrier on Ru(0001) surfaces of the unconventional phases can be evidently reduced through a synergistic role of crystal phases and strain. Therefore, crystal phase engineering offers efficient approaches for the rational design of noble metal nanocatalysts

to improve the chemical activity of electrochemical ammonia synthesis.

COMPUTATIONAL DETAILS

The calculations were performed using the density functional theory (DFT) method implemented in the Vienna ab initial Simulation Package (VASP).[54] The projector augmented wave (PAW) method was used to describe electron−ion interactions, and the gradient-corrected Perdew−Burke−Ernzerh (GGA-PBE) functional was used to determine electron exchange and correlation energy.[55,56] The cutoff energy for the plane-wave basis set was 500 eV. All close-packed surfaces are modeled by a six-layer symmetric periodic slab (see Figure S1). We used a p(3 × 3) supercell in the lateral plane and 15 Å of vacuum to separate the periodic slab in the z-direction in order to eliminate interactions in between. Four layers in the bottom were fixed, while the top two atoms were fully relaxed in all the structure optimization calculations. We used 15 × 15 × 9 and 5 × 5 × 1 Monkhorst−Pack k-point meshs for the lattice parameters' optimization of bulk phases and the adsorption/dissociation of N_2 on p(3 × 3) Ru surfaces, respectively. The convergence criterion of the electronic self-consistent calculation is 10^{-5} eV, and the force convergence for structural relaxation is less than 0.03 eV/Å on each unfixed atom. The empirical correction method, DFT-D3,[57] was adopted to describe van der Waals (vdW) interactions to obtain the accurate adsorption energies and reaction barriers of N_2 on Ru surfaces. The barriers for N_2 dissociation were calculated using the Climbing Image Nudged Elastic Band (CI-NEB) technique,[58−61] combined with the dimer method.[62]

ASSOCIATED CONTENT

ⓢ Supporting Information

The Supporting Information is available free of charge at https://pubs.acs.org/doi/10.1021/acsomega.1c06400.

Computational details for crystal phase stability. Figure S1: Surface slab models for adsorption and dissociation of adsorbates on Ru surfaces. Figure S2: Correlation between the length of the a (or b) axis and the interplanar spacing. Figure S3: Energy per atom as a function of the interplanar spacing. Figure S4: Correlation between the d/a ratio and the interplanar spacing. Figure S5: Energy per atom as a function of the d/a ratio value. Figure S6: PDOS of Ru d states on 2H(0001), 3C(111), 4H(0001), DHCP(0001), $6H_1(0001)$, and $6H_2(0001)$ surfaces. Figure S7: Geometries of the initial states, transition states, and final states in the N_2 decomposition process on strained and novel crystal phase surfaces. Adsorption energies for N and N_2 on strained and novel crystal phase surfaces, distance between the surface and N, and bond length of N_2 in the decomposition process. Figure S8: PDOS of Ru d states (black line) and the electronic states of N (red line) on the DHCP $(0001)_c$ surface. Figure S9: PDOS of Ru d states (black line) and the electronic states of N_2 (red line) in the TS on the DHCP $(0001)_c$ surface. Figure S10: Correlation between the N adsorption energy and the adsorption energy of N2 in the IS. Figure S11: Correlation between the IS N_2 adsorption energy and the adsorption energy of N_2 in the TS. Figure S12: Correlation between the IS N_2 adsorption energy and the adsorption energy of N_2 in

the FS. Figure S13: Correlation between the N adsorption energy and the adsorption energy of N_2 in the FS. Figure S14: Correlation between the N adsorption energy and the dissociation barrier of N_2. Figure S15: Correlation between the N adsorption energy and the adsorption energy of N_2 in the TS. Figure S16: Relationship between the dissociation barriers and the reaction energies for the dissociation of N_2 on strained surfaces and unconventional crystal phases. Table S1: Position of the d-band center of the 2H Ru strained structures and the novel Ru crystal phases referred to the Fermi level (in eV). Table S2: Adsorption energy of dissociative N_2 in the FS state for the strained and novel crystals. (PDF)

■ AUTHOR INFORMATION

Corresponding Author

Dingwang Yuan − *College of Materials Science and Engineering, Hunan University, Changsha 410082, China;* ⊙ orcid.org/0000-0002-7273-704X; Email: dwyuan@ hnu.edu.cn

Authors

Tuanping Xie − *College of Materials Science and Engineering, Hunan University, Changsha 410082, China*

Jing Zhou − *College of Materials Science and Engineering, Hunan University, Changsha 410082, China*

Li Cai − *College of Materials Science and Engineering, Hunan University, Changsha 410082, China*

Wangyu Hu − *College of Materials Science and Engineering, Hunan University, Changsha 410082, China*

Bowen Huang − *College of Materials Science and Engineering, Hunan University, Changsha 410082, China;* ⊙ orcid.org/ 0000-0002-2682-9584

Complete contact information is available at:
https://pubs.acs.org/10.1021/acsomega.1c06400

Notes

The authors declare no competing financial interest.

■ ACKNOWLEDGMENTS

■ REFERENCES

(1) Klerke, A.; Christensen, C. H.; Nørskov, J. K.; Vegge, T. Ammonia for hydrogen storage: challenges and opportunities. *J. Mater. Chem.* **2008**, *18*, 2304−2310.

(2) Wang, L.; Xia, M.; Wang, H.; Huang, K.; Qian, C.; Maravelias, C. T.; Ozin, G. A. Greening Ammonia toward the Solar Ammonia Refinery. *Joule* **2018**, *2*, 1055−1074.

(3) Shipman, M. A.; Symes, M. D. Recent progress towards the electrosynthesis of ammonia from sustainable resources. *Catal. Today.* **2017**, *286*, 57−68.

(4) Van der Ham, C. J.; Koper, M. T.; Hetterscheid, D. G. Challenges in reduction of dinitrogen by proton and electron transfer. *Chem. Soc. Rev.* **2014**, *43*, 5183−5191.

(5) Kyriakou, V.; Garagounis, I.; Vasileiou, E.; Vourros, A.; Stoukides, M. Progress in the Electrochemical Synthesis of Ammonia. *Catal. Today.* **2017**, *286*, 2−13.

(6) Zhou, F.; Azofra, L. M.; Ali, M.; Kar, M.; Simonov, A. N.; McDonnell Worth, C.; Sun, C.; Zhang, X.; MacFarlane, D. R. Electro-

synthesis of ammonia from nitrogen at ambient temperature and pressure in ionic liquids. *Energy Environ. Sci.* **2017**, *10*, 2516−2520.

(7) Suryanto, B. H. R.; Du, H. L.; Wang, D.; Chen, J.; Simonov, A. N.; MacFarlane, D. R. Challenges and prospects in the catalysis of electroreduction of nitrogen to ammonia. *Nat. Catal.* **2019**, *2*, 290−296.

(8) Foster, S. L.; Bakovic, S. I. P.; Duda, R. D.; Maheshwari, S.; Milton, R. D.; Janik, M. J.; Renner, J. N.; Greenlee, L. F. Catalysts for nitrogen reduction to ammonia. *Nat. Catal.* **2018**, *1*, 490−500.

(9) Strait, R. Grassroots success with KAAP. *Nitrogen Methanol* **1999**, *238*, 37−43.

(10) Jacobsen, C. J.; Dahl, S.; Hansen, P. L.; Törnqvist, E.; Jensen, L.; Topsøe, H.; Prip, D. V.; Møenshaug, P. B.; Chorkendorff, I. Structure sensitivity of supported ruthenium catalysts for ammonia synthesis. *J. Mol. Catal. Chem.* **2000**, *163*, 19−26.

(11) Tuba, R.; Nagyházi, M.; Turczel, G.; Balla, A.; Szálas, G.; Tóth, I.; Gál, G.; Bombicz, P.; Anastas, P. Towards Sustainable Catalysis - Highly Efficient Olefin Metathesis in Protic Media Using Phase Labelled Cyclic Alkyl Amino Carbene (CAAC) Ruthenium Catalysts. *ChemCatChem* **2020**, *12*, 1953−1957.

(12) Casey Stevens, C. A.; Lambie, S. G.; Ruffman, C.; Skúlason, E.; Garden, A. L. Geometric and Electronic Effects Contributing to N_2 Dissociation Barriers on a Range of Active Sites on Ru Nanoparticles. *J. Phys. Chem. C* **2019**, *123*, 30458−30466.

(13) Chakraborty, I.; Carvalho, D.; Shirodkar, S. N; Lahiri, S.; Bhattacharyya, S.; Banerjee, R.; Waghmare, U.; Ayyub, P. Novel hexagonal polytypes of silver: growth, characterization and first-principles calculations. *J. Phys.: Condens. Matter* **2011**, *23*, 325401.

(14) Vieira, L.; Possato, L.; Chaves, T.; Lee, J.; Sulmonetti, T.; Jones, C.; Martins, L. Insights into Redox Dynamics of Vanadium Species Impregnated in Layered Siliceous Zeolitic Structures during Methanol Oxidation Reactions. *ChemCatChem.* **2020**, *12*, 2.

(15) Chen, Y.; Lai, Z.; Zhang, X.; Fan, Z.; He, Q.; Tan, C.; Zhang, H. Phase engineering of nanomaterials. *Nat. Rev. Chem.* **2020**, *4*, 243−246.

(16) Kusada, K.; Kitagawa, H. A Route for Phase Control in Metal Nanoparticles: A Potential Strategy to Create Advanced Materials. *Adv. Mater.* **2016**, *28*, 1129−1142.

(17) Luo, M.; Guo, S. Strain-controlled electrocatalysis on multimetallic nanomaterials. *Nat. Rev. Mater.* **2017**, *2*, 17059.

(18) Mavrikakis, M.; Hammer, B.; Nørskov, J. K. Effect of Strain on the Reactivity of Metal Surfaces. *Phys. Rev. Lett.* **1998**, *81*, 2819−2822.

(19) Li, L.; Abild Pedersen, F.; Greeley, J.; Nørskov, J. K. Surface Tension Effects on the Reactivity of Metal Nanoparticles. *J. Phys. Chem. Lett.* **2015**, *6*, 3797−3801.

(20) Chen, Q.; Cheng, T.; Fu, H.; Zhu, Y. Crystal phase regulation in noble metal nanocrystals. *Chin. J. Catal.* **2019**, *40*, 1035−1056.

(21) Zhao, M.; Xia, Y. Crystal-phase and surface-structure engineering of ruthenium nanocrystals. *Nat. Rev. Mater.* **2020**, *5*, 440−459.

(22) Ramsdell, L. S. Studies on silicon carbide. *Am. Mineral.* **1947**, *32*, 64−82.

(23) Sow, C.; Mettela, G.; Kulkarni, G. U. Noble Metal Nanomaterials with Nontraditional Crystal Structures. *Annu. Rev. Mater. Res.* **2020**, *50*, 345−370.

(24) Yao, Y.; He, D.; Lin, Y.; Feng, X.; Wang, X.; Yin, P.; Hong, X.; Zhou, G.; Wu, Y.; Li, Y. Modulating fcc and hcp Ruthenium on the Surface of Palladium-Copper Alloy through Tunable Lattice Mismatch. *Angew. Chem.* **2016**, *55*, 5501−5505.

(25) Fan, Z.; Chen, Y.; Zhu, Y.; Wang, J.; Li, B.; Zong, Y.; Han, Y.; Zhang, H. Epitaxial growth of unusual 4H hexagonal Ir, Rh, Os, Ru and Cu nanostructures on 4H Au nanoribbons. *Chem. Sci.* **2017**, *8*, 795−799.

(26) Kitchin, J. R.; Nørskov, J. K.; Barteau, M. A.; Chen, J. G. Role of Strain and Ligand Effects in the Modification of the Electronic and Chemical Properties of Bimetallic Surfaces. *Phys. Rev. Lett.* **2004**, *93*, 156801.

(27) Fan, Z.; Zhang, H. Crystal phase-controlled synthesis, properties and applications of noble metal nanomaterials. *Chem. Soc. Rev.* **2016**, *45*, 63−82.

(28) Liu, S.; Li, Y.; Shen, W. Tuning the catalytic behavior of metal nanoparticles: The issue of the crystal phase. *Chin. J. Catal.* **2015**, *36*, 1409−1418.

(29) Xia, Z.; Guo, S. Strain engineering of metal-based nanomaterials for energy electrocatalysis. *Chem. Soc. Rev.* **2019**, *48*, 3265−3278.

(30) Ye, H.; Wang, Q.; Catalano, M.; Lu, N.; Vermeylen, J.; Kim, M. J.; Liu, Y.; Sun, Y.; Xia, X. Ru Nanoframes with an fcc Structure and Enhanced Catalytic Properties. *Nano Lett.* **2016**, *16*, 2812−2817.

(31) Lu, Q.; Wang, A.; Gong, Y.; Hao, W.; Cheng, H.; Chen, J.; Li, B.; Yang, N.; Niu, W.; Wang, J.; et al. Crystal phase-based epitaxial growth of hybrid noble metal nanostructures on 4H/fcc Au nanowires. *Nat. Chem.* **2018**, *10*, 456−461.

(32) Li, W. Z.; Liu, J. X.; Gu, J.; Zhou, W.; Yao, S. Y.; Si, R.; Guo, Y.; Su, H. Y.; Yan, C. H.; Li, W. X.; Zhang, Y. W.; Ma, D. Chemical Insights into the Design and Development of Face-Centered Cubic Ruthenium Catalysts for Fischer−Tropsch Synthesis. *J. Am. Chem. Soc.* **2017**, *139*, 2267−2276.

(33) Zheng, Y.; Jiao, Y.; Zhu, Y.; Li, L. H.; Han, Y.; Chen, Y.; Jaroniec, M.; Qiao, S. Z. High Electrocatalytic Hydrogen Evolution Activity of an Anomalous Ruthenium Catalyst. *J. Am. Chem. Soc.* **2016**, *138*, 16174−16181.

(34) Wu, T.; Sun, M.; Huang, B. Strain modulation of phase transformation of noble metal nanomaterials. *InfoMater.* **2020**, *2*, 715−734.

(35) Zhong, L.; Li, S. Crystal phase effect upon O_2 activation on gold surfaces through intrinsic strain. *Nanoscale.* **2019**, *11*, 14587−14591.

(36) Zheng Johansson, J. X.; Eriksson, O.; Johansson, B. Systematic behavior of the hexagonal axial ratio for the d transition metals. *Phys. Rev. B* **1999**, *59*, 6131−6138.

(37) Belonoshko, A. B.; Li, S.; Ahuja, R.; Johansson, B. High-pressure crystal structure studies of Fe, Ru and Os. *J. Phys. Chem. Solids.* **2004**, *65*, 1565−1571.

(38) Sheppard, D.; Xiao, P.; Chemelewski, W.; Johnson, D. A generalized solid-state nudged elastic band method. *J. Chem. Phys.* **2012**, *136*, 074103.

(39) Xiao, P.; Henkelman, G. Communication: From graphite to diamond: Reaction pathways of the phase transition. *J. Chem. Phys.* **2012**, *137*, 101101.

(40) Xiao, P.; Cheng, J. G.; Zhou, J. S.; Goodenough, J. B.; Henkelman, G. Mechanism of the $CaIrO_3$ post-perovskite phase transition under pressure. *Phys. Rev. B* **2013**, *88*, 144102.

(41) Khorshidi, A.; Violet, J.; Hashemi, J.; A.Peterson, A. How strain can break the scaling relations of catalysis. *Nat. Catal.* **2018**, *1*, 263−268.

(42) Wang, L.; Zeng, Z.; Gao, W.; Maxson, T.; Raciti, D.; Giroux, M.; Pan, X.; Wang, C.; Greeley, J. Tunable intrinsic strain in two-dimensional transition metal electrocatalysts. *Science* **2019**, *363*, 870−874.

(43) Zhao, M.; Figueroa Cosme, L.; Elnabawy, A. O.; Vara, M.; Yang, X.; Roling, L. T.; Chi, M.; Mavrikakis, M.; Xia, Y. Synthesis and Characterization of Ru Cubic Nanocages with a Face-Centered Cubic Structure by Templating with Pd Nanocubes. *Nano Lett.* **2016**, *16*, 5310−5317.

(44) Ruban, A.; Hammer, B.; Stoltze, P.; Skriver, H.; Nørskov, J. Surface electronic structure and reactivity of transition and noble metals1Communication presented at the First Francqui Colloquium, Brussels, 19−20 February 1996.1. *J. Mol. Catal. Chem.* **1997**, *115*, 421−429.

(45) Bennich, P.; Wiell, T.; Karis, O.; Weinelt, M.; Wassdahl, N.; Nilsson, A.; Nyberg, M.; Pettersson, L. G. M.; Stöhr, J.; Samant, M. Nature of the surface chemical bond in N_2 on Ni(100) studied by x-ray-emission spectroscopy and ab initio calculations. *Phys. Rev. B* **1998**, *57*, 9274−9284.

(46) Pettersson, L.; Nilsson, A. A Molecular Perspective on the d-Band Model: Synergy Between Experiment and Theory. *Top. Catal.* **2014**, *57*, 2−13.

(47) Mortensen, J.; Morikawa, Y.; Hammer, B.; Nørskov, J. K. Density Functional Calculations of N_2 Adsorption and Dissociation on a Ru(0001) Surface. *J. Catal.* **1997**, *169*, 85−92.

(48) Wang, S.; Petzold, V.; Tripkovic, V.; Kleis, J.; Howalt, J. G.; Skúlason, E.; Fernández, E. M.; Hvolbæk, B.; Jones, G.; Toftelund, A.; et al. Universal transition state scaling relations for (de)hydrogenation over transition metals. *Phys. Chem. Chem. Phys.* **2011**, *13*, 20760−20765.

(49) Munter, T. R.; Bligaard, T.; Christensen, C. H.; Nørskov, J. K. BEP relations for N_2 dissociation over stepped transition metal and alloy surfaces. *Phys. Chem. Chem. Phys.* **2008**, *10* (34), 5202−5206.

(50) Dahl, S.; Logadottir, A.; Egeberg, R. C.; Larsen, J. H.; Chorkendorff, I.; Törnqvist, E.; Nørskov, J. K. Role of Steps in N_2 Activation on Ru(0001). *Phys. Rev. Lett.* **1999**, *83*, 1814−1817.

(51) Li, J.; et al. Atomically dispersed manganese catalysts for oxygen reduction in proton-exchange membrane fuel cells. *Nat. Catal.* **2018**, *1*, 935−945.

(52) Andersen, M.; Levchenko, S. V.; Scheffler, M.; Reuter, K. Beyond Scaling Relations for the Description of Catalytic Materials. *ACS Catal.* **2019**, *9*, 2752−2759.

(53) Li, H.; Liu, Y.; Chen, K.; Margraf, J. T.; Li, Y.; Reuter, K. Subgroup Discovery Points to the Prominent Role of Charge Transfer in Breaking Nitrogen Scaling Relations at Single-Atom Catalysts on VS_2. *ACS Catal.* **2021**, *11*, 7906−7914.

(54) Kresse, G.; Furthmüller, J. Efficient iterative schemes for ab initio total-energy calculations using a plane-wave basis set. *Phys. Rev. B* **1996**, *54*, 11169−11186.

(55) Blöchl, P. E. Projector augmented-wave method. *Phys. Rev. B* **1994**, *50*, 17953−17979.

(56) Perdew, J. P.; Burke, K.; Ernzerhof, M. Generalized Gradient Approximation Made Simple. *Phys. Rev. Lett.* **1996**, *77*, 3865−3868.

(57) Lundqvist, B. I.; Andersson, Y.; Shao, H.; Chan, S.; Langreth, D. C. Density functional theory including Van Der Waals forces. *Int. J. Quantum Chem.* **1995**, *56*, 247−255.

(58) Schenter, G. K.; Mills, G.; Jónsson, H. Reversible work based quantum transition state theory. *J. Chem. Phys.* **1994**, *101*, 8964−8971.

(59) Henkelman, G.; Uberuaga, B. P.; Jónsson, H. A climbing image nudged elastic band method for finding saddle points and minimum energy paths. *J. Chem. Phys.* **2000**, *113*, 9901−9904.

(60) Henkelman, G.; Jónsson, H. Improved tangent estimate in the nudged elastic band method for finding minimum energy paths and saddle points. *J. Chem. Phys.* **2000**, *113*, 9978−9985.

(61) Mills, G.; Jónsson, H.; Schenter, G. K. Reversible work transition state theory: application to dissociative adsorption of hydrogen. *Surf. Sci.* **1995**, *324*, 305−337.

(62) Henkelman, G.; Jónsson, H. A dimer method for finding saddle points on high dimensional potential surfaces using only first derivatives. *J. Chem. Phys.* **1999**, *111*, 7010−7022.